JCTC Journal of Chemical Theory and Computation

Article

pubs.acs.org/JCTC

Conformational Changes and Free Energies in a Proline Isomerase

Elena Papaleo,[†] Ludovico Sutto,[‡] Francesco Luigi Gervasio,[‡,§] and Kresten Lindorff-Larsen*[,†]

[†]Structural Biology and NMR Laboratory, Department of Biology, University of Copenhagen, Ole Maaløes Vej 5, DK-2200 Copenhagen, Denmark

[‡]Institute of Structural and Molecular Biology and [§]Department of Chemistry, University College London, London WC1H 0AJ, United Kingdom

Supporting Information

ABSTRACT: Proteins are dynamic molecules and their ability to adopt alternative conformations is central to their biological function. The structural and biophysical properties of transiently and sparsely populated states are, however, difficult to study and an atomic-level description of those states is challenging. We have used enhanced-sampling all-atom, explicit-solvent molecular simulations, guided by structural information from X-ray crystallography and NMR, to describe quantitatively the transition between the major and a minor state of Cyclophilin A, thus providing new insight into how dynamics can affect enzyme function. We calculate the conformational free energy between the two states, and comparison with experiments demonstrates a surprisingly high accuracy for both the wild type protein and a mutant that traps the protein in its alternative conformation. Our results demonstrate how the combination of state-of-the-art force fields and enhanced sampling methods can provide a detailed and quantitative description of the conformational changes in proteins such as those observed in Cyclophilin A.

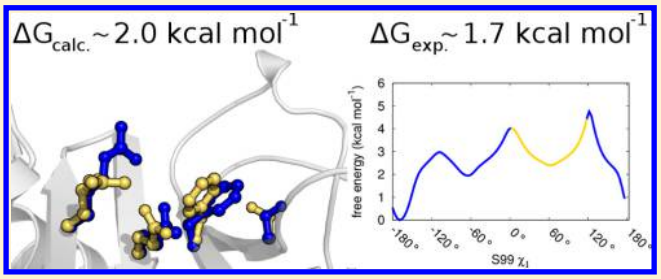

INTRODUCTION

Conformational dynamics can play a crucial role in protein function such as enzyme catalysis, molecular recognition, and cell signaling.[1,2] The conformations that can be attained by a protein can be described in terms of a rugged free-energy landscape,[3] where the global free energy minimum corresponds to the "ground" (major) state and where other local minima constitute alternative (minor) states for the protein.[1,4] The transient nature and low populations of such minor states challenge the limits of conventional structural biology methods as they cannot directly be observed, hence their alternative description as invisible or hidden states.[4]

From an experimental point of view, NMR spectroscopy has the unique ability to provide atomic-level data that reports on the motions in proteins over a wide range of time scales.[5] In particular, NMR relaxation dispersion experiments can in favorable cases provide structural information in the form of chemical shifts of minor states, which can in turn be used to derive structural models.[5,6] Also, new methods for the analysis of electron density maps from X-ray crystallography have provided insight into alternative conformations of proteins.[7] Despite this important progress, it is still far from routine to determine structural models and other properties of minor states in proteins, and their functional roles hence continue to be elusive.

Simultaneously with the development in experimental methods, improvements in the accuracy of molecular force fields[8−10] and in methods to achieve extensive sampling of biomolecular conformations[11−15] have increased the predictive ability of molecular dynamics (MD) simulations applied to biological problems.[16]

Here we examine the extent to which state-of-the-art simulation methods can capture accurately the conformational change in a protein. We focused our studies on Cyclophilin A (CypA), a proline isomerase, which has been the object of extensive experimental studies. NMR experiments have revealed that CypA undergoes millisecond motions during enzyme catalysis.[17] This motion is also observed in the free enzyme, where CypA may adopt at least two distinct conformations including a minor state that has a ∼6% population.[18] While previous computational studies on CypA have mostly focused on and provided insight into a potential link between protein motions and overall enzyme function,[19−24] we here instead aimed to investigate to what extent simulations can describe quantitatively the free energy surface of the free protein in solution.

A *Ringer* analysis of an electron density map of free CypA at room temperature[25] provided evidence for a concerted set of side chain motions involving Ser99, Phe113, Met61, and Arg55 (Figure 1). The conformational changes probed by NMR and crystallography were argued to be the same, and a mutation (S99T) designed on the basis of the Ringer analysis is able to trap CypA in its minor state, thus inverting the population of the two states.[25] The modified conformational dynamics in

Received: June 20, 2014
Published: August 20, 2014

   dx.doi.org/10.1021/ct500536r | J. Chem. Theory Comput. 2014, 10, 4169−4174

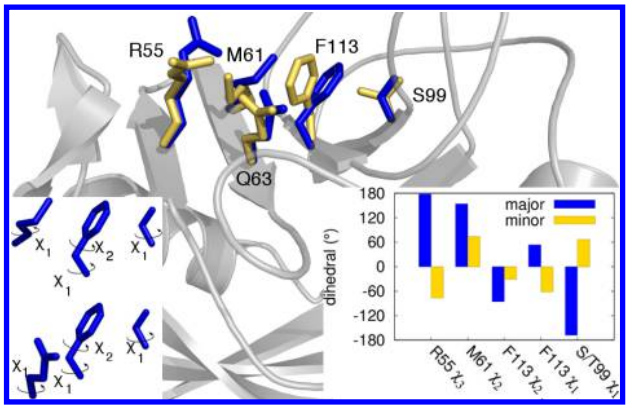

Figure 1. Dynamic network of residues in CypA. A previously identified[19] network of residues involved in a transition between a major and minor state is shown as sticks in (blue) wild type and (yellow) S99T CypA. The left insert highlights the side chain dihedrals that we have used as collective variables in the metadynamics simulations. As described in the main text, we used two different sets of CVs, termed $\chi_{S\text{-}F\text{-}M}$ and $\chi_{S\text{-}F\text{-}Q}$, which are illustrated in the two rows. The insert on the right shows the values of the relevant side chain dihedral angles that differ the most between the two states of CypA, and which we used as collective variables in our simulations. The dihedral angles were calculated from the structures of the wild type (major state) and S99T (minor state) protein. We throughout calculated the χ_1 dihedral of T99 using the C_γ atom, to make comparisons with the wild type protein clearer.

S99T causes a substantial drop in the enzyme turnover rate, though the detailed origin of this effect remains unclear.

The crystal structure of the S99T variant validated the structural model of the minor state from the Ringer analysis, and together these structures provide us with a unique opportunity to examine the extent to which MD simulations can capture the structure and thermodynamics of conformational change in proteins. We have therefore used parallel-tempering metadynamics calculations,[12] a method for enhanced sampling of MD simulations, together with several recently developed molecular force fields, to study the conformational change and associated free energy in CypA. Our results demonstrate that these simulations, at least in the case of CypA, can accurately capture the energetics associated with the conformational change, as well as the effects induced by the S99T mutation. Moreover, our results provide additional structural insight into the dynamic network of residues in CypA and possibly how this might affect the overall catalytic efficiency of the enzyme.

METHODS

Molecular Dynamics Simulations. The crystal structures of wild type (3K0N) and the S99T variant (3K0O) CypA[25] were used as starting structures for our simulations, in both cases retaining all crystallographic water molecules. The H92A mutant was modeled using Pymol (www.pymol.org).

Simulations were performed with Gromacs 4.5[26] with the PLUMED 1.3 plugin[27] for the metadynamics calculations. The proteins were solvated in a dodecahedral box (length: 1.0 nm) of tip3p water molecules,[28] and we used three different force fields for the protein (CHARMM22*,[29] CHARMM36,[30] and Amber ff99SB*-ILDN[9]). The van der Waals interactions were smoothly shifted to zero between 0.8 and 1.0 nm, and the long-range electrostatic interactions were calculated by the particle mesh Ewald algorithm[31] with a 0.12 nm mesh spacing combined with a switch function for the direct space between 0.8 and 1.0 nm. The system evolves in the canonical ensemble, coupled with a velocity-rescale thermostat,[32] and a time step of 2 fs.

Enhanced Sampling. We used PT-MetaD[12] in the well-tempered ensemble[33] to enhance sampling. In such simulations, sampling of the free energy surface is enhanced by adding a history-dependent potential to a set of collective variables and further enhanced by allowing for exchanges between different temperatures. We used the well-tempered ensemble approach to overcome the inherently problematic scaling properties of PT simulations with large number of atoms, which typically require many closely spaced temperatures to ensure sufficient energy overlap between adjacent replicas hence increasing the exchange rate. In this approach, a constant bias on the energy is added to each replica to increase the width of the energy distribution so that exchange is ensured even when using a more widely spaced temperature scheme.[33,34] We therefore used seven replicas (at 295, 298, 310, 325, 341, 358, and 376 K) where the width of the energy distribution (of all but the "neutral" 298 K replica) was increased as described previously.[35] All the replicas are subject to an additional biasing force through well-tempered metadynamics simulations in which a Gaussian of width 0.1 rad in all the four dimensions is deposited in the collective variable space every 4 ps, with an initial height of 0.5 kJ mol^{-1} and a bias factor of 4. The two sets of CVs used are described in the main text. See the SI for additional information about the simulations.

Paths of Communication. The shortest paths of communication between S99 and R55 were calculated from the unbiased MD simulations using the Protein Structure Network/Linear Mutual Information (PSN/LMI) method as described previously.[36] Briefly, the Cα LMI matrix was calculated by averaging over nonoverlapping windows of 5 ns, and using a cutoff of 0.4 to reduce noise and to discard residues that are weakly correlated. The I_{crit} value employed in our simulations was 2.6, calculated as previously described.[36,37] The PSN was calculated for each structure, and only edges present in at least half of the simulation frames were considered. The PSN, LMI, and PSN-LMI calculations were performed using WORDOM.[38]

RESULTS

Simulating a Conformational Change and Calculating Conformational Free Energies in CypA. The NMR-determined lifetimes of the major and minor states of CypA are around 17 and 1 ms, respectively.[18] Such a slow process is beyond the range of standard MD simulations. Indeed, we found that in short 0.5 μs unbiased MD simulations of both wild type and S99T CypA, performed with either of three different force fields (CHARMM22*, CHARMM36, Amber ff99SB*-ILDN), that the structures mostly remained close to the crystallographic structures (Figure S1).

We therefore employed parallel-tempering metadynamics (PT-MetaD) simulations in the well-tempered ensemble[12,33−35] to obtain a fully converged free energy surface (FES) describing the transition, while keeping the high accuracy and atomistic resolution afforded by the CHARMM22* force field. In such simulations, sampling is enhanced by adding a history-dependent biasing potential along a set of specified *collective variables* (CVs) and by coupling the simulations to a range of temperatures (see Methods).

dx.doi.org/10.1021/ct500536r | J. Chem. Theory Comput. 2014, 10, 4169−4174

To design the CVs we used existing structural information, though the resulting free-energy landscapes result solely from the (transferable) molecular force field and are not biased by any experimental data. More precisely, based on the structures of wild type and S99T mutant CypA, we designed two sets of CVs that use a combination of χ_1 and χ_2 dihedral angles to distinguish the different side chain conformations (left insert in Figure 1). The first set (A; also referred to as $\chi_{S\text{-}F\text{-}M}$) includes the χ_1 dihedral of S99 and F113, the χ_2 dihedral of F113 and χ_2 of M61. The second set (B; $\chi_{S\text{-}F\text{-}Q}$) has in common the first three side chain dihedral angles in $\chi_{S\text{-}F\text{-}M}$ but differs for the fourth one, which in this case is the χ_1 of Q63. The first set of CVs involves the dihedral angles that were originally proposed to be part of the dynamical network in CypA.[25] Our choice of the χ_1 dihedral in Q63 as an alternative CV was motivated by our observation (see below) that Q63 is part of a coupling network that includes S99 and the catalytic R55. The two sets of CVs performed comparably in our PT-MetaD simulations, converging to the same free energy surface when projected on identical CVs, and allowed us to observe repeated transitions between the major and minor states of CypA during the 0.4-μs long PT-MetaD simulations (see Table S1 for an overview of the simulations performed).

The ability to sample both the major and minor states in our simulations allowed us to calculate the free energy surface that describes the conformational landscape of CypA either as one-dimensional projections along individual CVs (Figures 2a and b) or as contour plots with two CVs (Figures 2c). The force field used (CHARMM22*) is able to capture the multiple basins that each residue can adopt. The main minimum for S99 corresponds to the trans (t) rotamer,[39] while the minus (m) and plus (p) rotamers correspond to local minima (Figure 2a). F113 has two main minima with the p rotamer being at a slightly lower energy than the m rotamer (Figure 2b). The two-dimensional free-energy surface provides a clearer view of the coupled motions of the two residues (Figure 2c). The main energy barrier separates the p rotamer of S99 from the t/m rotamers, and there is a coupling between S99 and F113, so that while F113 is able to sample both the m and p rotamers freely in the major state (S99 t/m rotamers), the side chain of F113 becomes almost fully locked into the m rotamer in the minor state.

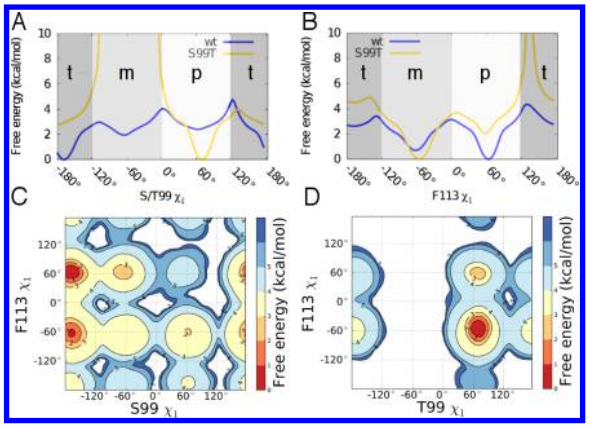

Figure 2. Free energy surfaces of CypA. The figure shows (A, B) one-dimensional and (C, D) two-dimensional free energy surfaces of the most important dihedral angles (the χ_1 of residues 99 and 113) as calculated by PT-MetaD simulations of both wild type and the S99T mutant of CypA. The profiles show clearly both the major and minor states of the wild type protein and how the S99T mutation stabilizes the minor state. The two-dimensional plots also demonstrate the energetic coupling between the two residues. The labels t/m/p refer to the trans, minus, or plus conformations of the side chain torsions.

By summing the populations across the free energy surface we computed the free energy difference between the major and minor states (Figure 3a). The free energy difference in the simulations of wild type CypA with CHARMM22* converges to ~2 kcal mol^{-1} after about 100 ns of sampling per replica and remains constant during the remainder of the simulation. The independent PT-MetaD run performed with the other set of CVs (set B) converges to the same free energy difference after 0.2 μs. Thus, the PT-MetaD simulations provide a well-converged estimate of the free energy difference. The converged nature of the simulations is also supported by the symmetric nature of the free energy surface along the χ_2 dihedral angle of F113 (Figure S2).

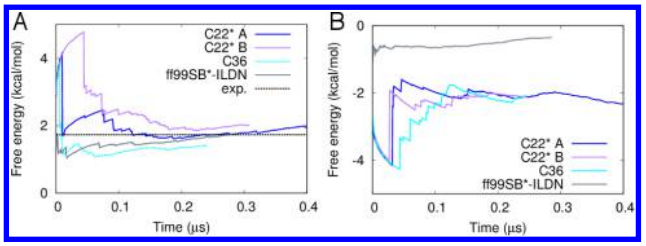

Figure 3. Precise and accurate conformational free energies calculated by PT-MetaD. The plots show the convergence of the free energy difference between the major and minor states in (A) wild type and (B) S99T mutant CypA. For each time point, the plots show the free energy difference calculated using the simulations up until that time. The dashed horizontal line in panel A marks the experimental value;[17] no comparable value is available for S99T. In these plots, the free energies were obtained by summing the populations in the major and minor states as quantified using the two-dimensional free energy surfaces in Figure 2 with the minor state being defined as having residue 99 in the p rotamer.

With converged simulations in hand it becomes meaningful to compare the calculated free energy differences to the corresponding experimental values. NMR relaxation dispersion experiments found the minor state to be populated at ~6%, corresponding to a free energy difference between major and minor states of 1.7 kcal mol^{-1}.[18] Thus, in addition to being precise, our simulations also appear to be surprisingly accurate.

Free Energy Landscape of the S99T CypA Mutant. We then proceeded to study the S99T variant of CypA, which was designed to trap the protein in the minor state conformation.[25] Crystallographic and NMR data on S99T demonstrated that it indeed adopts a (wild type) minor-like structure, and NMR relaxation dispersion experiments revealed that this protein also displays slow, millisecond motions thus suggesting that the populations of the two states had been inverted.[25]

We performed a set of PT-MetaD simulations of S99T using the same approach as for the wild type protein. The calculated free energy surfaces (Figures 2a and b) demonstrate that the free energies of the major and minor states have been inverted in the S99T mutant. In particular, we find that T99 is now mostly found in the p rotamer with a higher energy state at the t rotamer, and F113 also now has the m rotamer as its dominant conformation. The two-dimensional free energy surface of S99T (Figure 2d) indeed shows a clear free energy minimum around the crystallographically determined structure,

dx.doi.org/10.1021/ct500536r | J. Chem. Theory Comput. 2014, 10, 4169−4174

with a higher energy minor state with T99 in the t rotamer. The calculated free energy difference between the two states (Figure 3b) shows convergence after ∼100 ns, and again, we find good agreement between two independent simulations using the two sets of CVs (−2.6 and −2.4 kcal mol^{-1} for set A and B, respectively), confirming the ability of the simulations to quantitatively describe the transition. The free energy difference between the two states could not be measured accurately by relaxation dispersion experiments on S99T, though we note that the available NMR data suggests (in line with our observation) that the free energy difference in S99T is larger (and with opposite sign) than that in the wild type protein.

Force Field Dependency of the Free Energy Landscape. The choice of force field employed in a simulation can have a substantial impact on the results obtained.[8,9] It is therefore important that force fields are validated and benchmarked as widely as possible to ensure transferability to a wide range of applications. Our converged simulations enable us to perform such a validation, and we here compare the calculated conformational free energy landscapes resulting from CHARMM22* with those obtained with CHARMM36 and Amber ff99SB*-ILDN. All three force fields have recently been parametrized and shown to reproduce accurately the structural and dynamical parameters of a range of different protein and peptide systems.[9,30]

The simulations were performed using the $\chi_{S\text{-}F\text{-}M}$ set of CVs (set A) for both the wild type and S99T variant of CypA and compared to the simulations with CHARMM22* (Figures 2 and 4 and Figure S3). Reassuringly, all three force fields provide

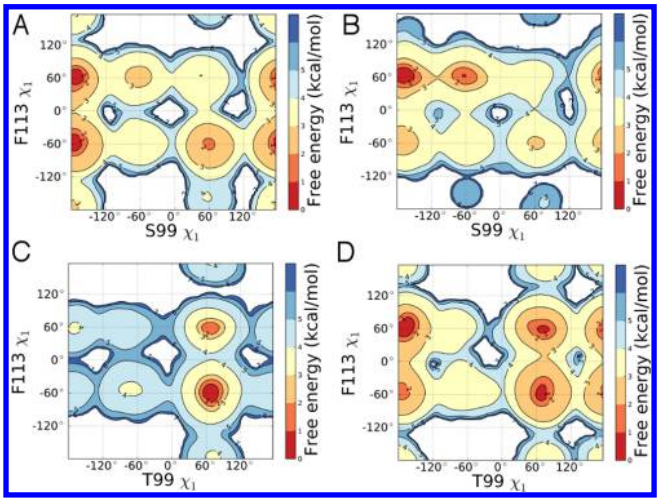

Figure 4. Effect of force field on the calculated free energy surfaces. The plots show the two-dimensional free energy surface obtained using either (A, C) CHARMM36 or (B, D) Amber ff99SB*-ILDN on (A, B) wild type or (C, D) S99T CypA. Together with the results from CHARMM22* (Figure 2), the results show that the free energy landscapes are relatively similar for the different force fields, with the noticeable exception that the free energy difference in S99T obtained with the Amber force field is substantially smaller than the value from the two CHARMM force fields (Figure 3).

a consistent view of the free energy landscape of CypA, with all force fields being able to sample both the major and minor states and capturing the population inversion in the S99T variant.

In the case of wild type CypA both the one-dimensional (Figure S3) and two-dimensional (Figures 2c and 4a and b) free-energy surfaces are relatively similar across the force fields, and all simulations give rise to free energy differences in very good agreement with experiments (Figure 3a).

In our simulations of S99T CypA we observe larger differences between the simulations performed with different force fields. In particular, while the two CHARMM force fields both show a relatively large free energy difference between the major and minor states, the Amber force field has the two states at comparable energies with the dominant conformation of S99T being only at a slightly lower free energy (0.5−1.0 kcal mol^{-1}) than the major conformation of the wild type protein (Figures 3b and 4c and d and Figure S4). Although the free energy difference could not be measured accurately by experiments, a very small free energy difference between the two states appears incompatible with the available experimental data. In particular, as the conformational exchange in S99T is in the slow exchange NMR regime,[25] two well-populated states would have shown up as two sets of peaks in the NMR spectra. We note that in the Amber simulation of S99T both rotamers of F113 are about equally populated even when T99 is in the p rotamer (Figure 4d and Figure S4). Thus, potentially the repulsive interactions between the two residues may be quantitatively different in the two force fields. This is also consistent with the fact that the two CHARMM force fields share nearly all parameters for nonbonded interactions (such as charges and van der Waals interactions) and mostly differ in the torsional degrees of freedom for the backbone and side chains. Moreover, we find that unbiased MD simulations with the Amber force field also reveals a less stable behavior of the two central CVs (Figure S1), suggesting perhaps that the CHARMM force fields overall provide the most accurate description of the conformational dynamics in CypA.

Dynamic Network in CypA Residues Exerting Its Effects Long-Range toward the Catalytic Site. Based on the similarity between the conformational exchange rate and the rate of catalysis, and the overlap between the residues involved in the dynamical process and those important in substrate binding, it is likely that the dynamical motions in CypA play a central role in the overall activity of the enzyme. Serine 99 plays a central role in the conformational change of CypA, and although it is located far away (C_α distance is ∼14 Å) from the catalytic R55, the S99T mutation has a substantial effect on the catalytic turnover rate.[25] It is thus of central interest to understand how the dynamics at S99 can exert its effects over longer ranges and help understand the molecular determinants that shape the free energy landscape.

In the major state, the side chain of S99 is well buried in the protein core, with a relative side chain solvent accessibility close to 0% and is involved in a network of hydrogen bonds that are present >70% of the time in our unbiased MD simulations of CypA. In particular, a hydrogen bond between the side chain hydroxyl of S99 and Nε in H92 is found when S99 is in the ground state and is almost fully occupied in the simulation. The network also includes additional hydrogen bonds between H92, T119, and D123. To assess the importance of this network in modulating the conformational preferences of the S99 side chain we performed a PT-MetaD simulation of a H92A mutant (Figure S4). Surprisingly, the free energy surfaces of the wild type and H92A proteins are very similar and result in similar free energy differences between major and minor states. Thus, it appears that a major state hydrogen bond between S99 and H92 is not a main determinant of the conformational free energy.

Originally, the χ_2 dihedral in M61 was tentatively assigned to be in the t and m rotamers in the major and minor states, respectively,[25] and was hypothesized to provide a link between S99/F113 and the catalytic arginine. Nevertheless, changes in the side chain rotamers of M61 were not obviously associated with the two states even in the analysis of the electron density from X-ray crystallography.[25] Our calculations suggest that free energy surfaces of the M61 χ_1 and χ_2 dihedral angles are essentially the same in wild type and S99T CypA, independently of the force field chosen (Figures S5 and S6). Moreover, there does not appear to be any strong coupling between the conformation of S99 and M61 in our simulations (Figures S5 and S6). We note that we find a similar result in simulations with CHARMM36 that has an improved set of side chain torsions for methionine and other amino acids[30] (Figure S7).

We therefore speculated whether the conformational dynamics of S99 could be coupled to R55, and hence overall enzyme function, via a mechanism that does not directly involve rotameric transitions in M61. In an attempt to identify suitable candidate pathways, we analyzed unbiased MD simulations of both wild type and S99T CypA using methods inspired by graph theory[36,37] to identify the shortest paths of communication between S99 and R55. Interestingly, we find that the most likely path that links F113 and R55 involves Q63, and not M61, with a 70% and 90% occurrence in wild type and S99T CypA, respectively. Moreover, NMR experiments also identified Q63 as one of the residues involved in the major conformational exchange process.[18] Glutamine 63 also interacts with the substrate forming hydrogen bonds,[21] and a very recent analysis of crystallographic data has shown it to be part of an allosteric network connecting the hydrophobic core to the active site of the protein.[40]

The importance of Q63 is also apparent from the reconstructed free-energy surfaces. The free energy surface of Q63 in the wild type protein shows that the t rotamer dominates with a substantial population also for the m rotamer (Figure 5). The S99T mutation appears to stabilize the m rotamer so that the populations of the t and m rotamers are roughly inverted in the mutant. The rotameric preferences of Q63 also appear to be weakly coupled to the rotameric state of S99 (Figure 5). Thus, the conformation of S99 and the effect of the S99T mutation, might affect function via perturbing Q63, which in turn could either affect substrate binding or the conformational properties in the catalytic site. These computational predictions might possibly be verified by experiments on Q63 mutants.

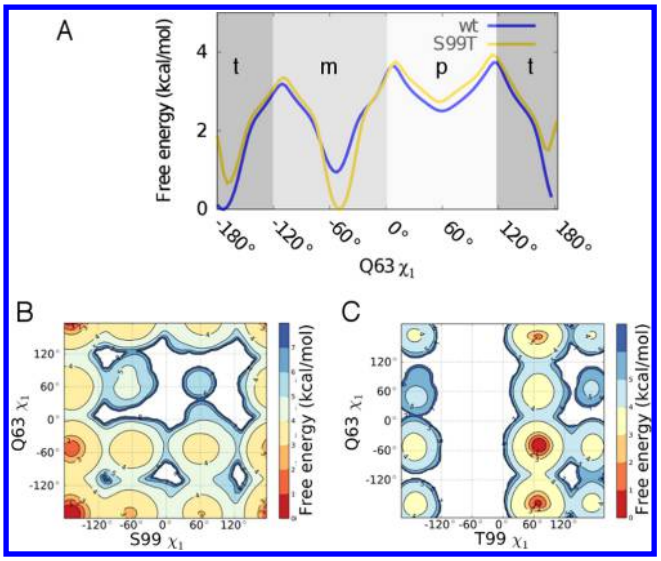

Figure 5. Coupling between residue 99 and Gln63 in CypA. (A) The free energy profiles along the χ1 dihedral angle in Q63 for both wild type and S99T CypA reveal that the altered conformational properties in S99T are propagated to Q63 located about ~10 Å away (C_α distance). The two-dimensional free energy profiles of χ1 of residues 63 and 99 in (B) wild type and (C) S99T mutant CypA further suggest a weak coupling between the two residues, which we speculate may play a role in the functional effect of the conformational dynamics and S99T mutation.

DISCUSSION

Conformational exchange plays an important role in protein biology and biophysics. Our results on CypA show that an enhanced sampling method together with current atomistic force fields has the potential to capture accurately the structure and energetics associated with a conformational change from a major (ground) state to a minor ("invisible") conformation in a protein. In particular, we were able to sample a slow conformational process in CypA and to calculate the associated free energy change with both high precision (i.e., from a converged simulation) and accuracy (close agreement with experiments). We also capture the substantial effects that result from the insertion of a single methylene group (S99T) in terms of structure and the change in the conformational free energy.

Recently, metadynamics approaches have for example been used to study slow conformational processes involved in allosteric signaling[41] and in the activation of kinases,[35] but in those cases it was more difficult to validate the calculated free energy surfaces. Although the results presented here relate to a slightly less complex conformational exchange process, they clearly show how well recently reparameterized force fields, when used together with enhanced sampling approaches, provide a quantitative insight into conformational energy landscapes of proteins.

Our data also sheds further light on how the conformational exchange in CypA might couple to the overall catalytic function of this enzyme. Our results suggest that the motions of S99 are coupled with Q63, a residue that both makes key hydrogen bond interactions with the substrate and interacts directly with the catalytic R55. Similarly, we find that the S99T mutation perturbs the conformational properties of Q63, though it is unclear whether this effect is the cause of the perturbed enzymatic function. The potential role of Q63 in the network of dynamically coupled residues has also recently been suggested using an automated analysis of atomic contacts in X-ray structures.[40]

In conclusion, our results demonstrate out how, at least in the case of CypA, the combination of state-of-the-art force fields and metadynamics approaches can provide a detailed and quantitative description of the conformational landscape that is both highly accurate and precise.

ASSOCIATED CONTENT

Supporting Information

Additional methods describing system setup, simulations, and analyses. Supporting results with additional free energy profiles. This material is available free of charge via the Internet at http://pubs.acs.org.

AUTHOR INFORMATION

Corresponding Author

*E-mail: lindorff@bio.ku.dk.

Notes

The authors declare no competing financial interest.

ACKNOWLEDGMENTS

E.P. and K.L.-L. were supported by a Hallas-Møller stipend from the Novo Nordisk Foundation (to K.L.-L.). The work was initiated under the HPC-EUROPA2 project with the support of the European Commission−Capacities Area−Research Infrastructure. We acknowledge that the results of this research have been achieved using the PRACE-2IP project (FP7 RI-283493) resource Rosa based in Switzerland at CSCS.

REFERENCES

(1) Boehr, D. D.; Nussinov, R.; Wright, P. E. *Nat. Chem. Biol.* **2009**, *5*, 789−96.
(2) Ramanathan, A.; Savol, A.; Burger, V.; Chennubhotla, C. S.; Agarwal, P. K. *Acc. Chem. Res.* **2014**, *47*, 149−56.
(3) Onuchic, J. N.; Wolynes, P. G. *Curr. Opin. Struct. Biol.* **2004**, *14*, 70−5.
(4) Baldwin, A. J.; Kay, L. E. *Nat. Chem. Biol.* **2009**, *5*, 808−14.
(5) Boehr, D. D.; Dyson, H. J.; Wright, P. E. *Chem. Rev.* **2006**, *106*, 3055−79.
(6) Neudecker, P.; Robustelli, P.; Cavalli, A.; Walsh, P.; Lundström, P.; Zarrine-Afsar, A.; Sharpe, S.; Vendruscolo, M.; Kay, L. E. *Science* **2012**, *336*, 362−6.
(7) Fraser, J. S.; Jackson, C. J. *Cell. Mol. Life Sci.* **2011**, *68*, 1829−41.
(8) Piana, S.; Klepeis, J. L.; Shaw, D. E. *Curr. Opin. Struct. Biol.* **2014**, *24C*, 98−105.
(9) Lindorff-Larsen, K.; Maragakis, P.; Piana, S.; Eastwood, M. P.; Dror, R. O.; Shaw, D. E. *PLoS One* **2012**, *7*, e32131.
(10) Best, R. B. *Curr. Opin. Struct. Biol.* **2012**, *22*, 52−61.
(11) Shaw, D. E.; Maragakis, P.; Lindorff-Larsen, K.; Piana, S.; Dror, R. O.; Eastwood, M. P.; Bank, J. A.; Jumper, J. M.; Salmon, J. K.; Shan, Y.; Wriggers, W. *Science* **2010**, *330*, 341−6.
(12) Bussi, G.; Gervasio, F. L.; Laio, A.; Parrinello, M. *J. Am. Chem. Soc.* **2006**, *128*, 13435−41.
(13) Sutto, L.; Marsili, S.; Gervasio, F. L. *Wiley Interdiscip. Rev. Comput. Mol. Sci.* **2012**, *2*, 771−779.
(14) Kohlhoff, K. J.; Shukla, D.; Lawrenz, M.; Bowman, G. R.; Konerding, D. E.; Belov, D.; Altman, R. B.; Pande, V. S. *Nat. Chem.* **2014**, *6*, 15−21.
(15) Harvey, M. J.; De Fabritiis, G. *Drug Discovery Today* **2012**, *17*, 1059−62.
(16) Dror, R. O.; Dirks, R. M.; Grossman, J. P.; Xu, H.; Shaw, D. E. *Annu. Rev. Biophys.* **2012**, *41*, 429−52.
(17) Eisenmesser, E. Z.; Bosco, D. A.; Akke, M.; Kern, D. *Science* **2002**, *295*, 1520−3.
(18) Eisenmesser, E. Z.; Millet, O.; Labeikovsky, W.; Korzhnev, D. M.; Wolf-Watz, M.; Bosco, D. A.; Skalicky, J. J.; Kay, L. E.; Kern, D. *Nature* **2005**, *438*, 117−21.
(19) Li, G.; Cui, Q. *J. Am. Chem. Soc.* **2003**, *125*, 15028−38.
(20) Ramanathan, A.; Agarwal, P. K. *PLoS Biol.* **2011**, *9*, e1001193.
(21) McGowan, L. C.; Hamelberg, D. *Biophys. J.* **2013**, *104*, 216−26.
(22) Doshi, U.; McGowan, L. C.; Ladani, S. T.; Hamelberg, D. *Proc. Natl. Acad. Sci. U. S. A.* **2012**, *109*, 5699−704.
(23) Camilloni, C.; Sahakyan, A. B.; Holliday, M. J.; Isern, N. G.; Zhang, F.; Eisenmesser, E. Z.; Vendruscolo, M. *Proc. Natl. Acad. Sci. U. S. A.* **2014**, *111*, 10203−8.
(24) Leone, V.; Lattanzi, G.; Molteni, C.; Carloni, P. *PLoS Comput. Biol.* **2009**, *5*, e1000309.
(25) Fraser, J. S.; Clarkson, M. W.; Degnan, S. C.; Erion, R.; Kern, D.; Alber, T. *Nature* **2009**, *462*, 669−73.
(26) Hess, B.; Kutzner, C.; van der Spoel, D.; Lindahl, E. *J. Chem. Theory Comput.* **2008**, *4*, 435−447.
(27) Bonomi, M.; Branduardi, D.; Bussi, G.; Camilloni, C.; Provasi, D.; Raiteri, P.; Donadio, D.; Marinelli, F.; Pietrucci, F.; Broglia, R. A.; Parrinello, M. *Comput. Phys. Commun.* **2009**, *180*, 1961−1972.
(28) Jorgensen, W. L.; Chandrasekhar, J.; Madura, J. D.; Impey, R. W.; Klein, M. L. *J. Chem. Phys.* **1983**, *79*, 926.
(29) Piana, S.; Lindorff-Larsen, K.; Shaw, D. E. *Biophys. J.* **2011**, *100*, L47−9.
(30) Best, R. B.; Zhu, X.; Shim, J.; Lopes, P. E. M.; Mittal, J.; Feig, M.; Mackerell, A. D. *J. Chem. Theory Comput.* **2012**, *8*, 3257−3273.
(31) Essmann, U.; Perera, L.; Berkowitz, M. L.; Darden, T.; Lee, H.; Pedersen, L. G. *J. Chem. Phys.* **1995**, *103*, 8577.
(32) Bussi, G.; Donadio, D.; Parrinello, M. *J. Chem. Phys.* **2007**, *126*, 014101.
(33) Bonomi, M.; Parrinello, M. *Phys. Rev. Lett.* **2010**, *104*, 190601.
(34) Deighan, M.; Bonomi, M.; Pfaendtner, J. *J. Chem. Theory Comput.* **2012**, *8*, 2189−2192.
(35) Sutto, L.; Gervasio, F. L. *Proc. Natl. Acad. Sci. U. S. A.* **2013**, *110*, 10616−21.
(36) Papaleo, E.; Lindorff-Larsen, K.; De Gioia, L. *Phys. Chem. Chem. Phys.* **2012**, *14*, 12515−25.
(37) Ghosh, A.; Vishveshwara, S. *Proc. Natl. Acad. Sci. U. S. A.* **2007**, *104*, 15711−6.
(38) Seeber, M.; Felline, A.; Raimondi, F.; Muff, S.; Friedman, R.; Rao, F.; Caflisch, A.; Fanelli, F. *J. Comput. Chem.* **2011**, *32*, 1183−94.
(39) Lovell, S. C.; Word, J. M.; Richardson, J. S.; Richardson, D. C. *Proteins* **2000**, *40*, 389−408.
(40) Van den Bedem, H.; Bhabha, G.; Yang, K.; Wright, P. E.; Fraser, J. S. *Nat. Methods* **2013**, *10*, 896−902.
(41) Palazzesi, F.; Barducci, A.; Tollinger, M.; Parrinello, M. *Proc. Natl. Acad. Sci. U. S. A.* **2013**, *110*, 14237−42.